

Enhanced Thermal Lens Effect in Gold Nanoparticle-Doped Lyotropic Liquid Crystal by Nanoparticle Clustering Probed by Z-Scan Technique

V. M. Lenart · R. F. Turchiello ·
G. F. Goya · S. L. Gómez

Received: 3 November 2014
© Sociedade Brasileira de Física 2015

Abstract This work presents an experimental study of the thermal lens effect in Au nanoparticles-doped lyotropic liquid crystals under cw 532 nm optical excitation. Spherical Au nanoparticles of about 12 nm were prepared by Turkevich's method, and the lyotropic liquid crystal was a ternary mixture of SDS, 1-DeOH, and water that exhibits an isotropic phase at room temperature. The lyotropic matrix induces aggregation of the nanoparticles, leading to a broad and a red-shifted surface plasmon resonance. The thermal nonlinear optical refraction coefficient n_2 increases as a power of number density of nanoparticles, being possible to address this behavior to nanoparticle clustering.

Keywords Thermal lens · Gold nanoparticles · Clustering · Lyotropic liquid crystal

1 Introduction

In the last years, there has been an increasing interest in the thermal and optical properties of nanocomposite materials because of the new phenomena arising from the nanoscale and the envisaged technological applications. In this field

stands out the nanofluids, stable suspensions of metallic nanoparticles whose optical properties arise from the surface plasmon resonance (SPR), a collective oscillation of the free electrons in the conduction band [1, 2]. An important feature of this band is its dependence on size [3] and shape [4, 5] of the nanoparticles and on the presence of clusters [6, 7]. Nanofluids also exhibit enhanced thermal transport properties [8–10]. Liquids with suspended nanoparticles display thermal conductivities significantly higher than that of the base fluids. Besides the numerous researches on the linear and nonlinear optical properties of noble metal nanoparticles, the photothermal properties of nanofluids have not deserved the same attention [11–13]. In addition to an interest in basic research, the study of the photothermal properties of nanofluids is relevant for technological and medical applications. In this sense, plasmonic photothermal therapy of tumors already is a promising new field in the nanomedicine [14, 15]. An important issue in nanofluids, envisaging practical applications, is the clustering [16, 17]. It was shown that the aggregation of Au nanoparticles leads to an enhancement in the heating effect under optical excitation [18] but a complete model about the generation and transport of heat taking into account the complex structure of the aggregates is lacking.

The aim of this paper is to give an insight into the role of nanoparticle clustering in the thermal nonlinear optical response of a medium containing gold nanoparticles (AuNPs), proposing a phenomenological model of the thermal conductivity and of the thermal lens effect. To this end, we have explored the formation of a thermal lens by the Z-scan technique in two different media containing spherical citrated gold nanoparticles, water, and lyotropic liquid crystal, varying nanoparticle concentration, under cw optical excitation at 532 nm.

S. L. Gómez (✉) · V. M. Lenart
Physics Department, State University of Ponta Grossa, Ponta Grossa, PR, Brazil
e-mail: sgomez@uepg.br

R. F. Turchiello
Physics Department, Federal University of Technology of Paraná, Ponta Grossa, PR, Brazil

G. F. Goya
Department of Condensed Matter Physics, Aragon Institute of Nanoscience, Zaragoza, Spain

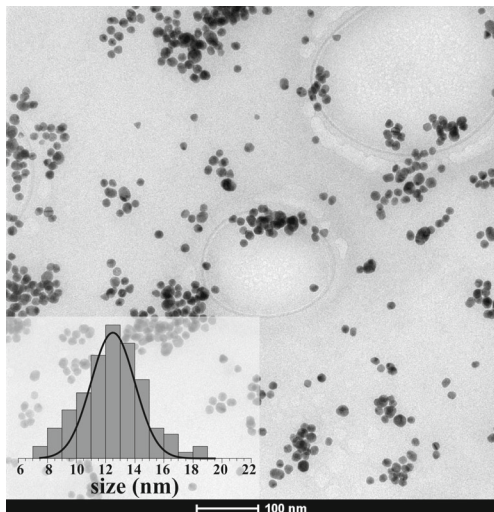


Fig. 1 Transmission Electron Microscopy image of the produced nanoparticles and the histogram of sizes distribution. The average size of the nanoparticles is about 12 nm

2 Experimental Details

For the synthesis of spheric Au nanoparticles, we used the standard Turkevich's method [19]. They used 20 ml of 1.0 mM of H ($\text{AuCl}_4 \cdot \text{H}_2\text{O}$) (Vetec PA) as precursor and 2.0 ml of a 1 % solution of $\text{Na}_3\text{C}_6\text{H}_5\text{O}_7 \cdot 2\text{H}_2\text{O}$ (Synth PA) as reductor and surfactant agent. These reagents were used without further purification. The temperature during the reaction was maintained close to 373 K. The half reactions for the synthesis of colloidal gold are given in (1) and (2).

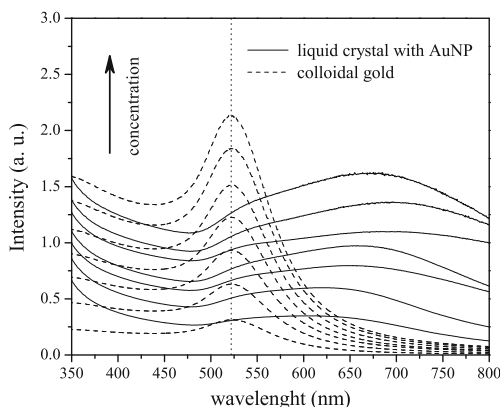
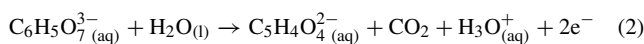


Fig. 2 UV-Vis absorption spectra of pure solutions of AuNPs (broken line) and AuNP-doped lyotropic liquid crystals (straight line) for different concentrations of AuNP

The result was a ruby red colloid. Measurements of zeta potential reveal that the nanoparticles are highly stable and have an average surface charge of -33.4 ± 0.5 mV at pH 8.2, which remained stable, protected from the light, for at least 5 months.

The lyotropic liquid crystal used in this study is a mixture of sodium dodecyl sulfate (SDS) [23 wt%], 1-decanol (1-DeOH) [2 wt%], and water [75 wt%], which exhibits an isotropic phase at room temperature (24 °C). The basic units of these kind of liquid crystals are the micelles, anisotropic aggregates of amphiphilic molecules, whose average dimensions have a typical size of $\sim 100\text{\AA}$ [20]. In the isotropic phase, the principal axes of the different anisotropic aggregates are oriented in space in a random way, i.e., the optical axis is not defined.

For both, colloidal gold and AuNP-doped lyotropic liquid crystal samples, named after colloid (C) and lyotropic (L), respectively, for shortness, we prepared seven dilutions of nanoparticles. The concentrations or number density (N) in particles/ml were $N_1(5.66 \times 10^{11})$, $N_2(8.49 \times 10^{11})$, $N_3(11.32 \times 10^{11})$, $N_4(14.15 \times 10^{11})$, $N_5(16.98 \times 10^{11})$, $N_6(19.8 \times 10^{11})$, and $N_7(22.64 \times 10^{11})$. These concentrations correspond to a filling factor of $\sim 10^{-5} - 10^{-4}\%$.

The following equipments were employed for characterizing the nanoparticles: Cary 50 from Varian (linear optical absorption), X-ray diffractometer Ultima IV from Rigaku (crystalline structure), Zetasizer Nano ZS90 from Malvern (zeta potential), TECNAI F30 (TEM), and Abbe refractometer RTA-100 (refraction index as a function of temperature).

2.1 The Z-scan Technique

The nonlinear optical properties of a medium at different time scales can be probed by the Z-scan technique [21], which exploits the formation of a lens with a variable focal length in a medium when illuminated by a tight Gaussian laser beam. Under incidence of a cw laser beam, the observed optical nonlinearity in a medium is essentially from thermal origin. A Gaussian laser induces a lens in an absorbing medium, named thermal lens, being possible to write the refraction index as $n = n_0 + (dn/dT)\Delta T$, where n_0 is the linear refraction index, dn/dT is the thermo-optic coefficient, and ΔT is the change in temperature [22]. Diffusion of heat leads to a spatial variation of the laser beam phase that does not match exactly its intensity spatial profile $I(r)$. However, for media with low optical absorption α and low thermal conductivity κ , the Sheik-Bahae's model [21], based in a purely local nonlinear optical effect, gives a good description of the transmittance in a Z-scan experiment for a thermal optical nonlinearity [23]. For a purely local nonlinear optical effect $n = n_0 + n_2 I$, where n_2 is the nonlinear refraction index. The magnitude and sign

of the fitting parameter of the Sheik-Bahae's model, n_2 , can be obtained by means of the closed-aperture Z-scan configuration. In this implementation, whose details are found elsewhere [24], the transmitted intensity by the sample of the focused laser is measured behind an iris centered along the z -axis at the far field as a function of the position of the sample around the focus. A medium characterized by $n_2 > 0$ (< 0) behaves like a positive (negative) lens. For a sufficiently thin sample, to first-order correction in the irradiance of a Gaussian laser beam, the normalized transmittance (Γ_c) is given by:

$$\Gamma_c = 1 - \frac{4\Phi \left(\frac{z}{z_o} \right)}{\left[1 + \left(\frac{z}{z_o} \right)^2 \right] \left[9 + \left(\frac{z}{z_o} \right)^2 \right]}, \quad (3)$$

where z_o is the Rayleigh range of the beam, $\Phi = kn_2 I_0 L_{ef}$, k is the wave number, $L_{ef} = [1 - \exp(-\alpha L)]/\alpha$ is the effective thickness of the sample, and I_0 is the irradiance at the beam waist ($z = 0$). For a thermal nonlinear optical response, it was shown [23] that:

$$n_2 \propto \frac{dn}{dT} \frac{\alpha}{\kappa}. \quad (4)$$

The signal of n_2 coincides with that of dn/dT . In this work, the samples were conditioned in 200 μm -thick glass cells and it was used a Gaussian cw laser at $\lambda = 532$ nm (Ventus, Laser Quantum). The beam waist at focus was 26 μm and data acquisition was made via oscilloscope (Tektronix, TDS1012B). The incident power on the sample was ~ 18 mW. This value is the threshold for the appearance of a thermal lens effect, within the sensitivity of our experimental apparatus, without unwanted hydrodynamical effects. It is worth to mention also that the characteristic formation time of a thermal lens in the aqueous colloid, i.e., the time to develop a stable refraction index gradient, is about 5 ms. A concomitant process in colloidal systems, in which a thermal gradient is established, is a mass diffusion process, named thermophoretic effect, with time scale in the order of seconds and that leads to a lens of matter. Within the sensibility of our experimental setup, it was not observed the formation of a lens of matter, so the optical response comes just from a thermal lens effect.

3 Results and Discussions

The nanoparticles have average size of about 12.5 ± 0.4 nm (Fig. 1). The absorption spectrum of the samples, the colloids, and the lyotropics for all the concentrations are shown in Fig. 2. The spectrum of the colloids displays the known narrow band of the SPR, picked at about 522 nm for all of them. Increasing the concentration, there is no evidence of clustering. On the other hand, the spectrum of the

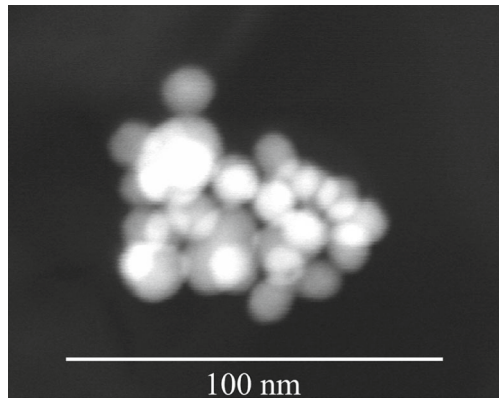


Fig. 3 CRYO-STEM-HAADF image of an aggregate of Au nanoparticles in the lyotropic liquid crystal matrix

lyotropics exhibits a broader and red-shifted SPR band, and the maximum of this band shifts to longer wavelengths when increasing N . This means that the average size of the clusters augments when N increases. Gaikwad et al. [25] ascribed to aggregates the origin of a broad band in the linear optical absorption of an AuNP-doped sponge phase. A possible mechanism that leads to agglomeration is the shielding of the negative charges on the surface of the AuNPs by ions Na^+ from the SDS, decreasing the electrostatic repulsion between the nanoparticles. Figure 3 shows a cryogenic scanning transmission electron microscopy in high angle annular dark field (CRYO-STEM-HAADF) image of a loosely packed aggregate with average radius $\langle r \rangle \sim 50$ nm found in the lyotropics. Esteban et al. showed that the structure of the absorption spectrum of an 3D cluster, grown under typical diffusion-limited aggregation conditions, can be understood as the contribution of different length resonant chains [7]. So, the actual spectrum of the lyotropics should be the contribution of AuNPs clusters of different shape. Also, at the excitation wavelength

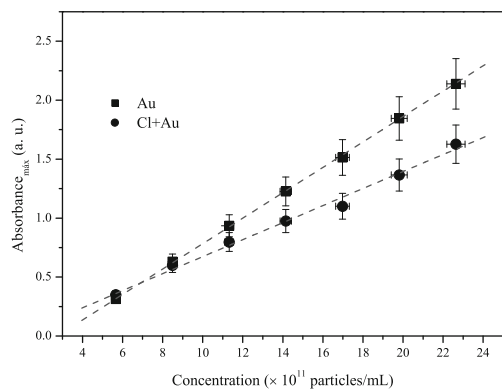


Fig. 4 Maximum of the SPR of the aqueous colloid of AuNPs (black square) and of the lyotropic liquid crystal doped with AuNPs (black circle) as a function of the concentration of AuNPs. The straight lines are guides for the eyes

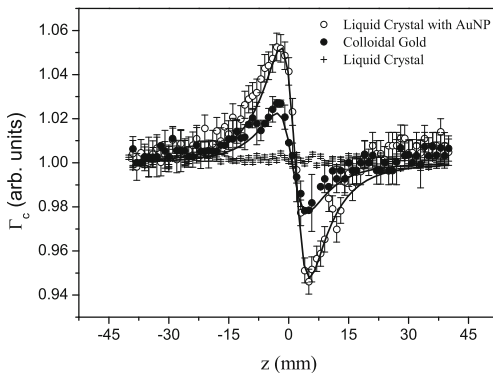


Fig. 5 Typical closed-aperture Z-scan curves for pure lyotropic liquid crystal (plus sign), pure colloidal gold (black circle), and AuNP-doped lyotropic liquid crystal (white circle). Continuous line indicates a fitting to (3)

(532 nm), the linear optical absorption of the AuNP-doped lyotropic increases linearly with N ($\alpha_L \propto N$) and for the same concentration of AuNPs, $\alpha_C \simeq 1.3 \alpha_L$ (Fig. 4). This may be ascribed to the red shift of the plasmon resonance due to the clustering of the nanoparticles.

Figure 5 shows typical closed-aperture Z-scan traces of AuNP-doped lyotropics, undoped lyotropic, and colloids, obtained at room temperature. The error bars correspond to the standard error of the mean of ten measurements in each z position. Colloids and lyotropics display a self-defocusing effect ($n_2 < 0$). Within the sensibility of our experimental setup, and for the beam, powers used in this work were not observed in the formation of a thermal lens in the undoped lyotropic liquid crystal. Yet, the empty glass cells do not show any thermal lens effect. Figure 6 shows the value of n_2 as a function of the number density of nanoparticles for the colloids and the lyotropics. It is worth to observe that the

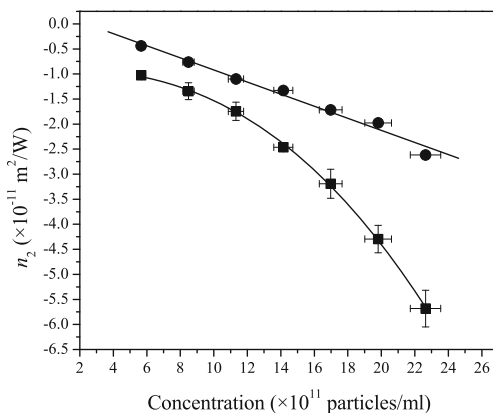


Fig. 6 Thermal nonlinear optical refraction n_2 as a function of concentration of nanoparticles of the colloid of AuNPs (black circle) and the AuNP-doped lyotropic liquid crystals (black square). Solid lines are a linear fitting for the colloid of AuNPs and a fitting to the function $a + b N^\beta$ for the AuNP-doped lyotropic liquid crystal

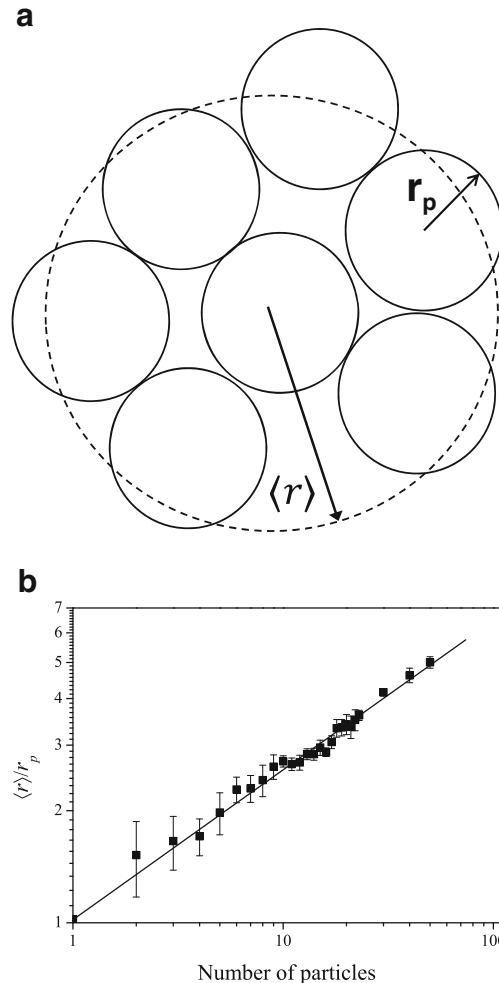


Fig. 7 **a** Sketch of a cluster of spheres of radius r_p packed randomly and the average sphere of radius $\langle r \rangle$. **b** Log-log graph of the average radius of the clusters of spheres as a function of the number N of spheres. The solid line is a linear fitting

intensity of the thermal lens depends linearly on the intensity of the laser beam (graph does not shown). So, we have employed the same power in all the samples. At the lower concentration $n_2^L \sim 2 n_2^C$, and a fitting of data show that $n_2^C \propto N$ and $n_2^L \propto N^{2.4}$ (solid lines in Fig. 6).

3.1 Dependence of κ and n_2 on Clustering

Shahriari et al. have observed previously for an aqueous dispersion of AuNPs under similar experimental conditions that $n_2 \propto N$ [26]. Lyotropic liquid crystals doped with superparamagnetic magnetite nanoparticles and ferrofluids exhibit the same behavior [27]. The relative magnitude of n_2 at lower concentration, i.e., for small aggregates, can be accounted for by the interplay between the thermo-optic coefficient, the effective thermal conductivity, and the optical absorption (see (4)) as follows: (1) for a similar ternary mixture of SDS, 1-DeOH, and water in the

isotropic phase $\frac{dn}{dT} \sim -2.7 \times 10^{-4} \text{ }^{\circ}\text{C}^{-1}$ [28] while for the colloids we obtained $\frac{dn}{dT} \sim -1.5 \times 10^{-4} \text{ }^{\circ}\text{C}^{-1}$; (2) the ratio between the linear optical coefficients of lyotropics and colloids is ~ 0.7 ; 3) for low filling factors the effective thermal conductivity is approximately that of the liquid medium [29], so for the aqueous dispersion of AuNPs $\kappa_C \simeq \kappa_{\text{water}} \simeq 0.6 \text{ W m}^{-1} \text{ K}^{-1}$ [30] and for the AuNP-doped lyotropic liquid crystal $\kappa_L \simeq \kappa_{\text{lyotropic}} \simeq 0.3 \text{ W m}^{-1} \text{ K}^{-1}$ [31]. The dependence of n_2 on the number density can be understood, at least qualitatively, by making the fundamental supposition that the average number of nanoparticles in the cluster (n^o) is proportional to N . The transfer of heat is mainly a surface phenomenon. Kumar et al. showed that for nanoparticles of radius r_p immersed in a liquid medium, the effective thermal conductivity $\kappa \propto \frac{1}{r_p}$ [29], i.e., $\kappa \propto \frac{S}{V}$, where S is the surface and V the volume of the nanoparticle. With regard to thermal conductivity, the aggregates behave like particles with increased value of S/V . To study the dependence of S/V on N , it was constructed an anisotropic aggregate of N identical beads packed randomly. To each new bead added to the aggregate, it was determined the mean radius $\langle r \rangle$ of the aggregate, averaging the linear dimension of the aggregate along three orthogonal directions (Fig. 7a). Figure 7b shows a log-log graph of the $\langle r \rangle$ in units of the radius of the beads (r_p) as a function of N . A linear fitting of data gives $\langle r \rangle \propto N^{0.4}$. Assuming for a cluster that $S = N 4\pi r_p^2$ and $V = \frac{4}{3}\pi \langle r \rangle^3$,

$$\kappa_L \propto \frac{S}{V} \propto \frac{N}{(N^{0.4})^3} = N^{-0.2}. \quad (5)$$

Measurements of the refraction index of our samples as a function of temperature (results not shown) for different concentrations of AuNPs show that $\frac{dn}{dT}$ is rather proportional to the concentration. Previous study showed a similar result [32]. So, taking into account that $\alpha_L \propto N$, and assuming that $\frac{dn}{dT} \propto N$, (4) gives

$$n_2^L \propto N \frac{N}{N^{-0.2}} \propto N^{2.2}, \quad (6)$$

where the exponent is very close to the value obtained experimentally.

4 Conclusions

In this work, we have showed that lyotropic liquid crystals doped with AuNPs have an optical absorption spectrum characterized by a broad red-shifted surface plasmon resonance, which can be explained by the formation of nanoparticle aggregates. The induced thermal lens for both media, aqueous dispersions of AuNPs and AuNP-doped lyotropic

liquid crystals, is negative ($n_2 < 0$). It is found experimentally that $n_2 \propto N$ for the aqueous dispersions of AuNPs and $n_2 \propto N^{2.4}$ for the AuNP-doped lyotropic liquid crystals. The nonlinear dependence of n_2 on N for the AuNP-doped lyotropic liquid crystals can be explained by a decrease of the surface to volume ratio of the loosely packed clusters when increase the number of particles in the aggregate. The theoretical value of the exponent, 2.2, is in good agreement to the experimental one.

Acknowledgments This work had the financial support of the Brazilian agencies CAPES, CNPq, FINEP, and Fundação Araucária, and it is part of the research program of the Instituto Nacional de Ciência e Tecnologia de Fluidos Complexos (INCT-FCx). The authors also thanks to the Advanced Microscopy Laboratory (LMA) of the Institute of Nanoscience of Aragon.

References

1. S.A. Maier, *Plasmonics: Fundamentals and applications* (Springer, New York, 2007)
2. M. Quinten, *Optical properties of nanoparticles systems: Mie and beyond* (Wiley-VCH, Singapore, 2011)
3. V. Juvé, M.F. Cardinal, A. Lombardi, A. Crut et al. *Nano. Lett.* **13**, 2234 (2013)
4. S. Link, M.B. Mohamed, M.A. El-Sayed. *J. Phys. Chem. B* **103**, 3073 (1999)
5. N.I. Grigorochuk. *Eur. Phys. J. B* **87**, 252 (2014)
6. A.L. Urban, X. Shen, Y. Wang, N. Large, M.W. Knight et al. *Nano. Lett.* **13**, 4399 (2013)
7. R. Esteban, R.W. Taylor, J.J. Baumberg. *J. Aizpurua, Langmuir* **28**, 8881 (2012)
8. C. Kleinstreuer, Y. Feng. *Nanoscale Res. Lett.* **6**, 229 (2011)
9. H. Xie, W. Yu, Y. Li, L. Chen. *Nanoscale Res. Lett.* **6**, 124 (2011)
10. J. Buongiorno, D. Venerus, N. Prabhat, T. McKrell, J. Townsend, R. Christianson, Y. Tolmachev, P. Kebinski et al. *J. Appl. Phys.* **106**, 094312 (2009)
11. R.F. Souza, M.A. Alencar, E.C. da Silva, M.R. Meneghetti, J.M. Hickmann. *Appl. Phys. Lett.* **92**, 201902 (2008)
12. H.I. Elim, J. Yang, J.Y. Lee. *Appl. Phys. Lett.* **88**, 083107 (2006)
13. B. Palpant, M. Rashidi-Huyeh, B. Gallas, S. Chenot, S. Fisson. *Appl. Phys. Lett.* **90**, 223105 (2007)
14. B.N. Khlebtsov, E.V. Panfilova, G.S. Terentyuk, I.L. Maksimova, A.V. Ivanov, N.G. Khlebtsov. *Langmuir* **28**, 8994 (2012)
15. J.L. Li, M. Gu. *IEEE J. Sel. Top. Quant.* **16**, 989 (2010)
16. D.O. Lapotko, E.Y. Lukianova-Hleb, A.A. Oraevsky. *Nanomedicine* **2**, 241 (2007)
17. K.V. Wong, M.J. Castillo. *Adv. Mech. Eng.* **2010**, 795478 (2010)
18. H.H. Richardson, Z.N. Hickman, A.O. Govorov, A.C. Thomas, W. Zhang, M.E. Kordesch. *Nano. Lett.* **6**, 783 (2006)
19. J. Turkevich, P.C. Stevenson, J. Hillier. *Discuss. Faraday Soc.* **11**, 55 (1951)
20. Y. Galerne, A.M. Figueiredo, L. Liébert. *J. Chem. Phys.* **87**, 1851 (1987)
21. M. Sheik-Bahae, A.A. Said, T.H. Wei, D.J. Hagan, E.W. Van Stryland. *IEEE J. Quantum Electron.* **26**, 760 (1990)
22. F. Simoni, *Nonlinear optical properties of liquid crystals and polymer dispersed liquid crystals* (World Scientific, Singapore, 1997)
23. F.L.S. Cuppo, A.M. Figueiredo Neto, S.L. Gómez, P. Palfy-Muhoray. *J. Opt. Soc. Am. B* **19**, 1342 (2002)

24. S.L. Gómez, F.L.S. Cuppo, A.M. Figueiredo Neto, T. Kosa, M. Muramatsu, R.J. Horowicz. *Phys. Rev. E* **59**, 3059 (1999)
25. A.V. Gaikwad, P. Verschuren, T. van der Loop, G. Rothenberg, E. Eiser. *Soft Matter.* **5**, 1994 (2009)
26. E. Shahriari, W.M.M. Yunus, K. Naghavi, Z.A. Talib. *Opt. Commun.* **283**, 1929 (2010)
27. F.L.S. Cuppo, S.L. Gómez, A.M. Figueiredo Neto. *Eur. Phys. J. E* **13**, 327 (2004)
28. J.R.D. Pereira, A.M. Mansanares, A.J. Palangana, M.L. Baesso, A.A. Barbosa, P.R.G. Fernandes. *Phys. Rev. E* **64**, 062701 (2001)
29. D.H. Kumar, H.E. Patel, V.R.R. Kumar, T. Sundararajan, T. Pradeep, S.K. Das. *Phys. Rev. Lett.* **93**, 144301 (2004)
30. CRC Handbook of Chemistry and Physics (CRC Press, Boca Raton, FL, 2003), 84th ed
31. F.L.S. Cuppo, A.M. Figueiredo Neto. *Langmuir* **18**, 9647 (2002)
32. R. Karimzadeh, N. Mansour. *Opt. Laser Technol.* **42**, 783 (2010)